physica status solidi rrl
www.pss-rapid.com

Impact of Sequential N Ion Implantation on Extended Defects and Mg Distribution in Mg Ion-Implanted GaN

Emi Kano, Jun Uzuhashi, Koki Kobayashi, Kosuke Ishikawa, Kyosuke Sawabe, Tetsuo Narita, Kacper Sierakowski, Michal Bockowski, Tadakatsu Ohkubo, Tetsu Kachi, and Nobuyuki Ikarashi*

In Mg ion implantation doping of GaN, sequential N ion implantation reportedly changes Mg concentrations in the Mg ion-implanted region and the underlying region after activation annealing. The impact of sequential N ion implantation on defects and Mg distribution after postimplantation annealing is investigated. The atomic-resolution analyses show that, in the Mg ion-implanted region, the N ion implantation increases the concentration of Mg_{Ga}. It is thus concluded that the Mg soluble in GaN by Mg ion implantation is increased by N ion implantation. The rest of the Mg atoms agglomerate to form clusters on the extended defects, and their concentration is also increased by the N implantation. The coarsening of extended defects is suppressed by the N ion implantation: the defects in the Mg+N-implanted sample are nanoscale interstitial-type defects, and they do not grow or annihilate after annealing. This indicates that the N implantation changes the concentrations of interstitials.

1. Introduction

Vertical GaN power devices have been developed as high-efficiency switching devices for high-power applications.[1–4] To unleash the full potential of such devices, selective area p-type doping is required, and Mg ion implantation processes have been developed for this purpose.[4–9]

A long-standing challenge with ion implantation doping for semiconductor devices is how to control the dopant distribution.[10–14] The outward diffusion of the dopants during postimplantation annealing lowers the dopant concentration in the implanted region and changes their concentration profile, which can be a severe restriction when designing device structures. Moreover, when fabricating the GaN devices, controlling the Mg distribution is a major challenge. A significant decrease in the Mg concentration in the ion-implanted region has been reported, especially in the high-concentration doping of Mg (typically, Mg concentration of about 1×10^{19} cm^{-3} or more)[8,9,15,16] that is used for forming the contact in the devices. The diffusion of Mg follows the diffusion equation and the distribution of Mg after 1300 °C annealing is documented in ref. [9].

Previous studies have shown that sequential N ion implantation after Mg ion implantation suppresses the lowering of the Mg concentration in the Mg-implanted region even after annealing.[16–18] This is presumably because, according to positron annihilation spectroscopy analysis, Mg atoms are distributed in accordance with the vacancies produced by the N ion implantation, thereby suppressing the outward diffusion of Mg. The previous analyses, however, did not take into account the effect of extended defects formed during annealing, which attract Mg atoms and can affect the Mg concentration profile.[9,19]

Transmission electron microscopy (TEM) analyses have indicated that the interstitial-type dislocation loops are formed in the initial stage of annealing and the vacancy-type dislocation loops are formed in the later stage.[19,20] The analyses have also indicated that, as the annealing duration increases, the small dislocation loops disappear (i.e., defect density decreases), while the size of the large dislocation loops increases.[21–23] The results also suggest that the evolution of the extended defects is dominated by the thermal diffusion of native defects.[19]

The purpose of our current study is to reveal the impact of Mg and N sequential ion implantation on the Mg distribution and acceptor formation after annealing, as well as the underlying mechanisms. To this end, we prepared Mg ion-implanted GaN crystals with and without N implantation and analyzed the

E. Kano, T. Kachi, N. Ikarashi
Institute of Materials and Systems for Sustainability
Nagoya University
Nagoya, Aichi 464-8601, Japan
E-mail: kano@imass.nagoya-u.ac.jp

J. Uzuhashi, T. Ohkubo
National Institute for Materials Science
Tsukuba 305-0047, Japan

K. Kobayashi, K. Ishikawa, K. Sawabe, M. Bockowski
Department of Electronics
Graduate School of Engineering
Nagoya University
Nagoya, Aichi 464-8603, Japan

T. Narita
Toyota Central R&D Labs., Inc.
Nagakute, Aichi 480-1192, Japan

K. Sierakowski, M. Bockowski
Institute of High Pressure Physics Polish Academy of Sciences
Sokolowska 29/37, 01-142 Warsaw, Poland

The ORCID identification number(s) for the author(s) of this article can be found under https://doi.org/10.1002/pssr.202400074.

DOI: 10.1002/pssr.202400074

crystallographic defects and Mg distribution at an atomic resolution using TEM and atom probe tomography (APT). The concentration of ion-implanted Mg and N was $1 \times 10^{19}\,cm^{-3}$. Our results show that the defects in these samples differ significantly. Furthermore, in the Mg-implanted region, the sequential N implantation increased both the number of Mg atoms distributed uniformly and the number of Mg atoms agglomerated to form clusters. The role of the defects in increasing the amount of the Mg atoms is discussed.

2. Results

The Mg ion-implanted GaN samples with and without sequential N implantation are referred to in the following as Mg + N-implanted and Mg-implanted samples, respectively. The sample preparation conditions are the same for both samples except for the N ion implantation. Undoped GaN epitaxial films were grown by metalorganic vapor phase epitaxy on free-standing GaN (0001) substrates. Mg ion implantation was performed to generate a 300 nm-thick box-shaped concentration profile with a concentration of $1 \times 10^{19}\,cm^{-3}$. The depth profile of the Mg concentration in the as-implanted sample is shown in **Figure 1**. N ion implantation was performed to generate the 300 nm-thick box-shaped profile with a concentration of $1 \times 10^{19}\,cm^{-3}$. We used the SRIM program to design the N concentration profile.[24] Annealing was performed in N_2 atmosphere of 1.0 GPa at 1300 °C for 30 min. This annealing condition is reportedly enough for activating Mg atoms doped by ion implantation.[25]

The structure and density of the extended defects were examined by annular dark-field (ADF) scanning TEM (STEM) at an acceleration voltage of 200 kV. The inner and outer angles of the ADF detector were set to 20 and 60 mrad, respectively. For atomic scale resolution, we used the high-angle ADF (HAADF) condition, where the inner and outer angles were set to 50 and 150 mrad, respectively. TEM specimens were prepared by mechanical thinning followed by Ar-ion milling. The TEM specimen thicknesses were determined by convergent beam electron diffraction (CBED) analysis using the Mbfit program.[26] The details of the thickness determination are provided in the supplemental material. Secondary ion mass spectrometry (SIMS) analysis was utilized to measure the distribution of Mg and H. In the present annealing process, H reportedly diffuses into GaN from the ambient to form a stable complex with Mg_{Ga}, and the concentration of H matches that of Mg_{Ga}.[9,27] Mg_{Ga}, a Mg atom at the Ga site, reportedly acts as an acceptor in GaN.[28] Three-dimensional Mg distributions were examined by APT. APT specimens were prepared using a focused ion beam milling, where the low energy ion beam at 2 keV was utilized in the final step to reduce the damage during the milling. APT measurements were performed with 250 kHz 355 nm UV laser pulsing at a specimen temperature of 30 K. The laser pulse energy was set to 10 fJ. Frequency distribution analysis was used to examine the local fluctuations in Mg concentration.[24,29]

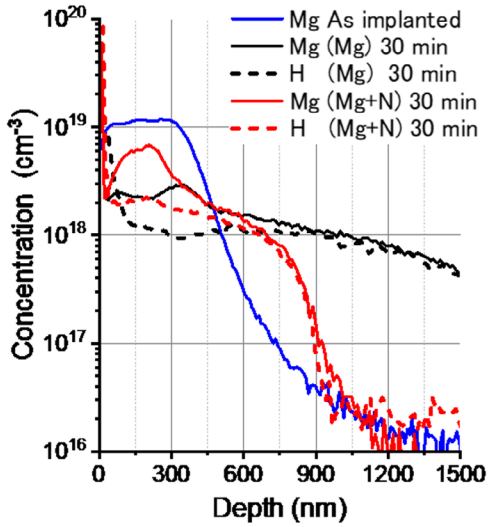

Figure 1. Concentration depth profiles of Mg and H after annealing. The profile in the as-implanted sample is also indicated. In the ion-implanted region (to the depth of 300 nm from the surface), both the total Mg concentration and H concentration are higher in the Mg + N-implanted sample (red solid and dotted lines) than in the Mg-implanted sample (black solid and dotted lines).

The SIMS results of the Mg concentrations measured in the samples are shown in Figure 1. The measured H concentrations, which represent the Mg_{Ga} concentrations, are also shown. A Mg concentration peak is observed in the ion implantation region (150–250 nm depth) of the Mg + N-implanted sample. The Mg concentration in the ion-implanted region is higher for the Mg + N-implanted sample than for Mg-implanted sample, which is consistent with previous reports.[16,17] Moreover, we found that the H concentration averaged over the depths from 150 to 250 nm is higher in the Mg + N-implanted sample than in the Mg-implanted sample, with concentrations of 2.1×10^{18} and $1.2 \times 10^{18}\,cm^{-3}$, respectively (**Table 1**). This result demonstrates that the sequential N implantation significantly increases the concentration of Mg_{Ga} in the Mg ion-implanted region.

ADF–STEM images of the Mg-implanted and Mg+N-implanted samples are shown in **Figure 2**a,b, respectively. In both micrographs. the incident beam direction is $<1\bar{1}00>$ and the TEM specimen thickness is 150 nm. The small bright dots and circles are the extended defects produced by the ion implantation and subsequent annealing. In the Mg-implanted sample, small bright dots and circles with 50 to 100 nm diameters were observed. The loops reportedly form during defect coarsening.[21,30] In contrast, in the Mg + N-implanted sample, we found a high density of small bright dots but no circles. These findings indicate that the coarsening is suppressed in the Mg + N-implanted sample.

Table 1. Concentrations of H and Mg. The concentrations of Mg_{Ga} (or H) in the Mg+N-implanted and Mg-implanted samples were measured by SIMS. The concentrations of uniformly distributed Mg and of Mg forming clusters were estimated from APT.

	Mg + N [$10^{18}\,cm^{-3}$]	Mg [$10^{18}\,cm^{-3}$]
H	2.1	1.2
Mg (uniformly distributed)	1.7	1.0
Mg (forming clusters)	2.5–4.4	0.8–2.5

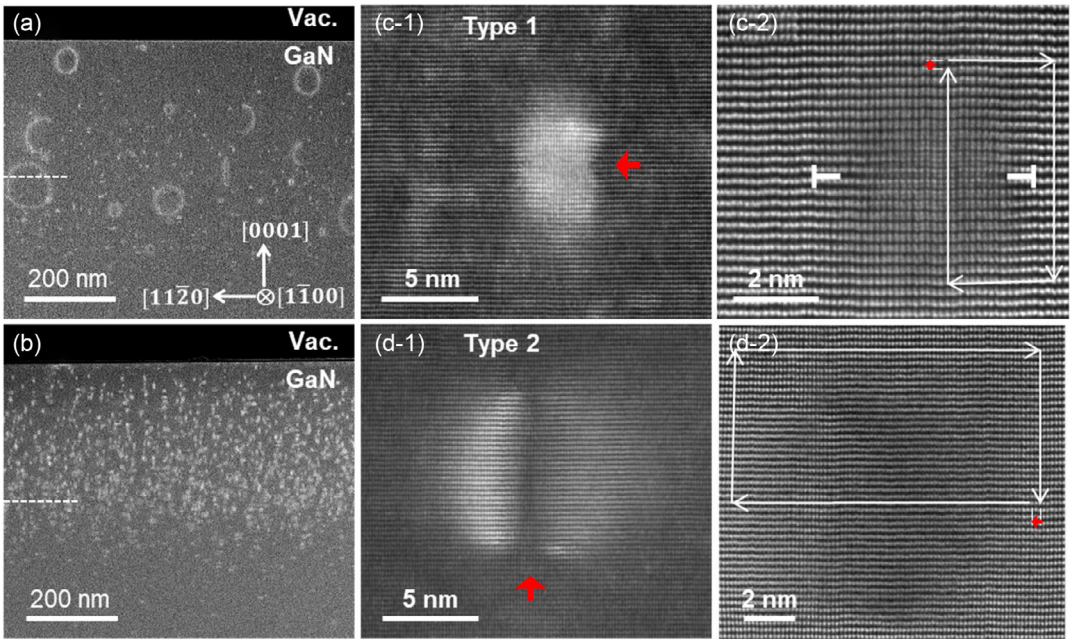

Figure 2. a) Cross-sectional ADF–STEM image of Mg-implanted sample and b) Mg + N-implanted sample. Bright circles and nanoscale dots are defects produced by the ion implantation and subsequent annealing. In (b), only nanoscale dots were observed. c) ADF–STEM and HAADF–STEM images of type 1 and d) type 2 defects in Mg + N-implanted samples, respectively. In (c-1), the defect is observed as a bright area with a central neck (arrowed). The Burgers circuit in (c-2) shows $b = \frac{1}{2}<0001>$ and the edge dislocation symbols indicate an extra c-plane. In (d-1), the defect is seen as a bright region divided into two sides by the dark region (arrowed). The Burgers circuit in (d-2) shows $b = \frac{1}{3}<11\bar{2}0>$, indicating that an extra a-plane is added to the defect.

The structural details of the defect in the Mg + N-implanted sample are shown in Figure 2c–d. Two types of defects with typical sizes of 3–10 nm are observed. Figure 2(c-1) and (c-2), respectively, shows the ADF–STEM and HAADF–STEM images of the defect denoted as type 1. In the ADF–STEM image, the defect is observed as a bright area with a central neck (arrowed). The HAADF–STEM image, where each bright dot shows an individual Ga atomic column, indicates that an extra atomic plane is inserted at the position indicated by the edge dislocation symbols. The Burgers circuit shows that the Burgers vector of the defect is $b = \frac{1}{2}<0001>$. These results indicate that the defect is an interstitial-type dislocation loop with an extra GaN c-plane. In addition, the bright area in Figure 2(c-1) represents the changes in the diffraction condition caused by the extra c-plane. Figure 2(d-1) and (d-2) respectively show the ADF–STEM and HAADF–STEM images of the defect denoted as type 2. In the ADF–STEM image, the defect is seen as a bright region divided into two sides by the dark region (arrowed). The Burgers circuit indicated on the HAADF–STEM image shows that $b = \frac{1}{3}<11\bar{2}0>$. These results indicate that the defect is an interstitial-type dislocation loop with an extra GaN a-plane. The interstitial-type dislocation loops with an extra a-plane or a c-plane are also found in Mg ion-implanted GaN (without N implantation) in the initial stage of annealing at 1300 °C (<30 min).[19,20] However, they grow and annihilate as the annealing progresses and are barely found at 30 min.[19] In contrast, the defects in the Mg + N-implanted sample remain unannihilated even after annealing for 30 min.

The volume density of the dislocation loops was $4.2 \pm 1.1 \times 10^{16}\,\mathrm{cm}^{-3}$ in the depth range of 150–250 nm from the sample surface. In this measurement, we counted the number of dislocation loops in a 100 nm square of the cross-sectional ADF–STEM images at a TEM specimen thickness of 50 nm. A thinner specimen is suitable for observing small defects since the background intensity of a TEM image decreases as the TEM specimen thickness decreases. In contrast, the number of defects per measurement area decreases as the specimen thickness decreases, thus increasing the standard deviation of the measured number of defects. Therefore, we opted to use 50 nm-thick TEM specimens for defect density measurement, and dislocation loops with an observed image size of 3 nm or larger were counted. The standard deviation is mainly due to the variation in the number of dislocation loops per measurement area.

We examined the Mg distribution in the Mg + N sample at an atomic resolution. **Figure 3**a shows the ADF–STEM image and (b) shows the Mg atom map by APT of the same specimen area. The bright dots in the STEM image show the dislocation loops and the green dots in the atom map show Mg atoms. The arrows in the STEM image and the atom map indicate the same position in the APT specimen, showing that Mg atoms agglomerate to form clusters at dislocation loops. Close-ups of the Mg atom map at type 1 and 2 defects are shown in Figure 3c,d, respectively. The atom maps show that the Mg clusters were flat doughnut-shaped and that the clusters at the type 1 defects were on the c-plane (i.e., (0001) plane) while those at the type 2 defects

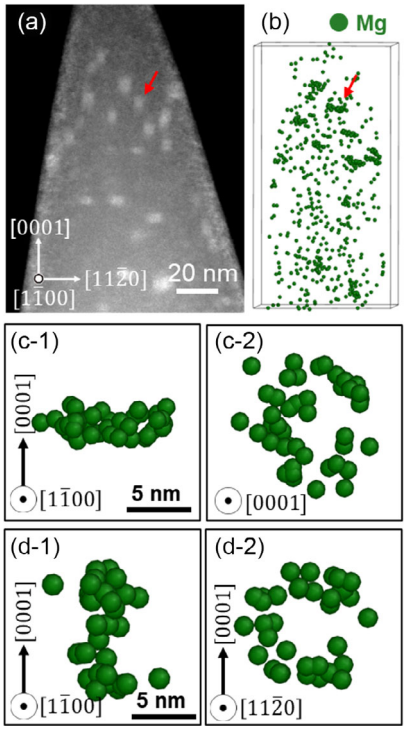

Figure 3. a) ADF–STEM and b) Mg atom map by APT of the same specimen area of the Mg + N-implanted sample. Green dots in b) show Mg atoms. Arrows indicate the same specimen position, showing that Mg forms clusters at dislocation loops. Close-ups of Mg clusters viewed in the orthogonal directions: (c-1), (c-2) cluster at type 1 defect and (d-1), (d-2) cluster at type 2 defect. Clusters are flat doughnut-shaped, and the cluster at the type 1 defect is on the c-plane while that at the type 2 defect is on the a-plane.

were on the a-plane (i.e., (11$\bar{2}$0) plane). These results indicate that Mg atoms agglomerate around the edges of the extra planes of the dislocation loops and that the strain fields generated by the extra planes attract Mg atoms to form clusters, as discussed in our previous work.[19] The APT results show that the average number of Mg atoms per flat doughnut-shaped cluster was 56.5.

Using the APT data, we classified Mg atoms in the Mg ion-implanted region as either clustered or uniformly distributed. Frequency distribution analysis was performed to estimate the concentration of uniformly distributed Mg atoms (see the supplemental material for details). The results are listed in Table 1. The concentration of Mg atoms forming clusters is obtained by subtracting that of uniformly distributed Mg atoms from that of total Mg atoms estimated from APT analysis. The concentration of the Mg atoms forming clusters varied slightly depending on the measurement area. This is mainly due to the small measurement volume of APT (typically 1×10^5 nm^3); that is, the number of Mg clusters, which affects the amount of the Mg atoms in the area, varies from one measurement area to another. The results in Table 1 indicate that the concentration of Mg atoms forming clusters is larger in the Mg + N-implanted sample than in the Mg-implanted sample. Moreover, the concentration of uniformly distributed Mg atoms is larger in the Mg + N-implanted sample than in the Mg-implanted sample. This strongly suggests that the concentration of Mg soluble in GaN is higher in the Mg + N-implanted sample compared to the Mg-implanted sample.

3. Discussion

These SIMS and APT analyses indicate that the concentration of H is comparable to that of uniformly distributed Mg atoms in each sample (Table 1). This suggests that the uniformly distributed Mg atoms occupy Ga sites (Mg_{Ga}) and that only a small part of Mg atoms in the clusters form stable complexes with H atoms. More importantly, the concentration of H in the Mg + N-implanted sample is remarkably higher than that in the Mg-implanted sample. Previous studies have indicated that the concentration of Mg soluble in GaN in doping by Mg ion implantation is 1.3×10^{18} cm^{-3} after postimplantation annealing,[15] which is comparable to the concentration of Mg_{Ga} and that of uniformly distributed Mg atoms in the Mg-implanted sample in the present experiment. Thus, these results indicate that the sequential N ion implantation increases the concentration of Mg soluble in GaN in doping by Mg ion implantation. Since Mg_{Ga} forms through the reaction between a Ga vacancy and a Mg atom, and since the N ion implantation forms Ga vacancies in addition to those produced by Mg implantation,[17] the increased Ga vacancy concentration in the Mg + N-implanted sample could be a cause for the increased Mg_{Ga} concentration in the sample.

Next, we estimated the percentage of Mg atoms agglomerated on the defects in the Mg forming cluster. The number of Mg atoms agglomerated at the dislocation loops in the Mg + N sample is given by the product of the dislocation loop density (4.2×10^{16} cm^{-3} in Figure 2b) and the number of Mg atoms per dislocation loop (56.5 in Figure 3); that is, 2.4×10^{18} cm^{-3}. This indicates that the amount of Mg atoms agglomerated at the dislocation loops accounts for more than half of that of the Mg atoms forming clusters ($2.5–4.4 \times 10^{18}$ cm^{-3}). In addition, dislocation loops that are smaller than those examined in our experiment (smaller than 3 nm) are also accompanied by a strain field and would cause Mg cluster formation. Therefore, we can conclude that the Mg agglomeration at the dislocation loops is the main cause for the Mg cluster formation in the Mg + N-implanted sample.

Our TEM analysis shows that small interstitial-type dislocation loops are observed in the Mg + N-implanted sample. This means that coarsening, i.e., annihilation and growth, of the dislocation loops was significantly suppressed. The annihilation and growth of the interstitial-type dislocation loops depend directly on the concentration of interstitials around the dislocation loops.[22,23] Namely, since the dislocation loop has an extra GaN a- or c-plane (Figure 2), the dislocation loop annihilates (grows) when both concentrations of N_i and Ga_i around the dislocation loop are below (above) the equilibrium concentration of the dislocation loop. Thus, the results observed in the Mg + N sample suggest that either the concentration of N_i or Ga_i is above the equilibrium concentration and that the other concentration is below it. Therefore, the results in Figure 2 indicate that the N ion implantation changed the concentrations of N_i and Ga_i in the Mg-implanted sample to suppress the annihilation and growth

of the nanoscale dislocation loops. The TEM analysis also shows that no vacancy-type dislocation loops were found in the Mg + N-implanted sample. We previously reported that a GaN a-plane is missing in a vacancy-type dislocation loop in Mg ion-implanted GaN,[20] which indicates that the same number of V_{Ga} and V_N are needed to form the vacancy-type dislocation loop. Furthermore, the sequential N ion implantation reportedly reduces the concentration of V_N,[18] while it increases the concentration of V_{Ga} in the Mg ion-implanted GaN.[16,17] Thus, in the present experiment, the sequential N implantation might reduce the concentration of V_N to suppress the formation of vacancy-type dislocation loops.

4. Conclusion

We investigated the impact of sequential N ion implantation on defects and Mg distribution in Mg ion-implanted GaN after post-implantation annealing at 1300 °C for 30 min. The concentration of ion-implanted Mg and N was 1×10^{19} cm^{-3}. Atomic-resolution analyses performed in the Mg ion-implanted region showed that the concentrations of both uniformly distributed Mg atoms and Mg_{Ga} are increased by the N ion implantation. In addition, these concentrations coincide with each other in the Mg + N-implanted and Mg-implanted samples. We thus conclude that the Mg soluble in GaN by Mg ion implantation was increased by the N ion implantation. The increased solubility can be attributed to the increased V_{Ga} by the N implantation. Our analyses also indicate that the rest of the Mg atoms formed clusters on the extended defects and that the amount of these Mg atoms was increased by the N ion implantation. We found that the coarsening of extended defects was suppressed by the N ion implantation: the defects in the Mg + N-implanted sample were nanoscale interstitial-type defects, and they did not grow or annihilate after annealing. This indicates that the N implantation changed the concentrations of interstitials, which in turn affected the coarsening of the defects. Furthermore, no vacancy-type extended defects were observed in the Mg + N-implanted sample, which suggests that the concentration of V_N is reduced by the N implantation.

Supporting Information

Supporting Information is available from the Wiley Online Library or from the author.

Acknowledgements

The authors would like to thank Prof. Koh Saito of Nagoya University and Prof. Kenji Tsuda of Tohoku University for their invaluable discussions on the CBED measurement of specimen thickness. Part of this work was supported by the MEXT "Program for Research and Development of Next-Generation Semiconductor to Realize Energy-Saving Society" (JPJ005357) and the "Program for Creation of Innovative Core Technology for Power Electronics" (JPJ009777).

Conflict of Interest

The authors declare no conflict of interest.

Data Availability Statement

The data that support the findings of this study are available from the corresponding author upon reasonable request.

Keywords

GaN, Mg, N ion-implantation, transmission electron microscopy

Received: March 7, 2024
Revised: April 7, 2024
Published online: April 22, 2024

[1] T. Oka, T. Ina, Y. Ueno, J. Nishii, *Appl. Phys. Express* **2015**, *8*, 6.
[2] R. Tanaka, S. Takashima, K. Ueno, H. Matsuyama, M. Edo, *Jpn. J. Appl. Phys.* **2020**, *59*, SGGD02.
[3] J. Liu, M. Xiao, R. Zhang, S. Pidaparthi, H. Cui, A. Edwards, M. Craven, L. Baubutr, C. Drowley, Y. Zhang, *IEEE Trans. Electron Devices* **2021**, *68*, 2025.
[4] T. Kachi, T. Narita, H. Sakurai, M. Matys, K. Kataoka, K. Hirukawa, K. Sumida, M. Horita, N. Ikarashi, K. Sierakowski, M. Bockowski, J. Suda, *J. Appl. Phys.* **2022**, *132*, 130901.
[5] J. C. Zolper, M. H. Crawford, S. J. Pearton, C. R. Abernathy, C. B. Vartuli, C. Yuan, R. A. Stall, *J. Electron. Mater.* **1996**, *25*, 839.
[6] B. N. Feigelson, T. J. Anderson, M. Abraham, J. A. Freitas, J. K. Hite, C. R. Eddy, F. J. Kub, *J. Cryst. Growth* **2012**, *350*, 21.
[7] H. Iguchi, T. Narita, K. Kataoka, M. Kanechika, A. Uedono, *J. Appl. Phys.* **2019**, *126*, 125102.
[8] H. Sakurai, M. Omori, S. Yamada, Y. Furukawa, S. Hideo, T. Narita, K. Kataoka, M. Horita, M. Bockowski, J. Suda, T. Kachi, *Appl. Phys. Lett.* **2019**, *115*, 142104.
[9] H. Sakurai, T. Narita, M. Omori, S. Yamada, A. Koura, M. Iwinska, K. Kataoka, M. Horita, N. Ikarashi, M. Bockowski, J. Suda, T. Kachi, *Appl. Phys. Express* **2020**, *13*, 086501.
[10] J. Mayer, *Ion Implantation in Semiconductors: Silicon and Germanium*, Academic Press, Cambridge, Massachusetts, **1970**.
[11] E. Rimini, *Ion Implantation: Basics to Device Fabrication*, Springer, Berlin, Germany, **1994**.
[12] L. Pelaz, M. Jaraiz, G. H. Gilmer, H. J. Gossmann, C. S. Rafferty, D. J. Eaglesham, J. M. Poate, *Appl. Phys. Lett.* **1997**, *70*, 2285.
[13] H. Mehrer, *Diffusion in Solids: Fundamentals, Methods, Materials, Diffusion-Controlled Processes*, Springer Series in Solid-State Sciences, New York City, **2007**.
[14] T. Narita, H. Yoshida, K. Tomita, K. Kataoka, H. Sakurai, M. Horita, M. Bockowski, N. Ikarashi, J. Suda, T. Kachi, Y. Tokuda, *J. Appl. Phys.* **2020**, *128*, 090901.
[15] T. Narita, A. Uedono, T. Kachi, *Phys. Status Solidi B* **2022**, *259*, 2200235.
[16] A. Uedono, R. Tanaka, S. Takashima, K. Ueno, M. Edo, K. Shima, K. Kojima, S. F. Chichibu, S. Ishibashi, *Sci. Rep.* **2021**, *11*, 20660.
[17] A. Uedono, H. Sakurai, J. Uzuhashi, T. Narita, K. Sierakowski, S. Ishibashi, S. F. Chichibu, M. Bockowski, J. Suda, T. Ohkubo, N. Ikarashi, K. Hono, T. Kachi, *Phys. Status Solidi B* **2022**, *259*, 2200183.
[18] K. Shima, R. Tanaka, S. Takashima, K. Ueno, M. Edo, K. Kojima, A. Uedono, S. Ishibashi, S. F. Chichibu, *Appl. Phys. Lett.* **2021**, *119*, 182106.
[19] E. Kano, K. Kataoka, J. Uzuhashi, K. Chokawa, H. Sakurai, A. Uedono, T. Narita, K. Sierakowski, M. Bockowski, R. Otsuki, K. Kobayashi, Y. Itoh, M. Nagao, T. Ohkubo, K. Hono, J. Suda, T. Kachi, N. Ikarashi, *J. Appl. Phys.* **2022**, *132*, 065703.
[20] K. Iwata, H. Sakurai, S. Arai, T. Nakashima, T. Narita, K. Kataoka, M. Bockowski, M. Nagao, J. Suda, T. Kachi, N. Ikarashi, *J. Appl. Phys.* **2020**, *127*, 105106.

[21] T. Nakashima, E. Kano, K. Kataoka, S. Arai, H. Sakurai, T. Narita, K. Sierakowski, M. Bockowski, M. Nagao, J. Suda, T. Kachi, N. Ikarashi, *Appl. Phys. Express* **2021**, *14*, 011005.
[22] C. Bonafos, D. Mathiot, A. Claverie, *J. Appl. Phys.* **1998**, *83*, 3008.
[23] B. Burton, M. V. Speight, *Philos. Mag. A* **1986**, *53*, 385.
[24] J. F. Ziegler, M. D. Ziegler, J. P. Biersack, *Nucl. Instruments Methods Phys. Res., Sect. B* **2010**, *268*, 1818.
[25] K. Hirukawa, K. Sumida, H. Sakurai, H. Fujikura, M. Horita, Y. Otoki, K. Sierakowski, M. Bockowski, T. Kachi, J. Suda, *Appl. Phys. Express* **2021**, *14*, 056501.
[26] K. Tsuda, M. Tanaka, *Acta Crystallogr., Sect. A Found. Crystallogr.* **1999**, *55*, 939.
[27] K. Sumida, K. Hirukawa, H. Sakurai, K. Sierakowski, M. Horita, M. Bockowski, T. Kachi, J. Suda, *Appl. Phys. Express* **2021**, *14*, 121004.
[28] J. Neugebauer, C. G. Van De Walle, *J. Appl. Phys.* **1999**, *85*, 3003.
[29] A. Kumar, J. Uzuhashi, T. Ohkubo, R. Tanaka, S. Takashima, M. Edo, K. Hono, *J. Appl. Phys.* **2019**, *126*, 235704.
[30] E. Kano, R. Otsuki, K. Kobayashi, K. Kataoka, K. Sierakowski, M. Bockowski, M. Nagao, T. Narita, T. Kachi, N. Ikarashi, *Phys. Status Solidi RRL* **2023**, *17*, 2300035.